Journal of Nuclear Materials 442 (2013) S119–S123
DOI: http://dx.doi.org/10.1016/j.jnucmat.2012.12.034

Tensile and fracture characteristics of oxide dispersion strengthened Fe–12Cr produced by hot isostatic pressing

Vanessa de Castro *, Jose Maria Garces-Usan, Teresa Leguey, Ramiro Pareja

Departamento de Física, Universidad Carlos III de Madrid, Avda. de la Universidad 30, 28911 Leganés, Madrid, Spain

Abstract: The mechanical characteristics of a model oxide dispersion strengthened (ODS) alloy with nominal com-position Fe–12 wt%Cr–0.4 wt%Y_2O_3 were investigated by means of microhardness measurements, tensile tests up to fracture in the temperature range of 298–973 K, and fracture surface analyses. A non-ODS Fe–12 wt%Cr alloy was also studied to assess the real capacity of the oxide dispersion for strengthening the alloy. The materials were produced by mechanical alloying followed by hot isostatic pressing consolida-tion and heat treatment at 1023 K. The strengthening effect of the oxide nanodispersion was effective at all temperatures studied, although the tensile strength converges towards the one obtained for the ref-erence alloy at higher temperatures. Moreover, the ODS alloys failed prematurely at $T < 673$ K due to the presence of Y-rich inclusions, as seen in the fracture surface of these alloys.

1. Introduction

Reduced activation ferritic–martensitic and ferritic steels (RAFMS and RAFS) with Cr contents ~9–12 and 13–18 wt% are the reference structural materials for the first wall and breeding blanket of future fusion reactors. During their service-life, RAFMS and RAFS will be subjected to extreme conditions including very high temperatures and radiation damage coming from the 14 MeV neutrons generated by the fusion reactions [1]. RAFMS/RAFS have an operating temperature limited to ~823 K due to their low creep rupture strength above this temperature [2,3]. Reinforc-ing these steels with stable nanometer-sized Y-rich oxide particles could enhance the efficiency of a reactor by raising the upper oper-ating temperature by at least 100 K, while the swelling and radia-tion resistance of RAFMS/RAFS appears to be superior to austenitic steels [4,5]. The particles seem to inhibit dislocation recovery and recrystallization up to ~973 K, improving the mechanical behaviour at high temperature. Oxide nanoparticles also provide a high density of sinks for irradiation induced point defects and He. This would reduce irradiation hardening and restrain the formation of He bubbles at grain boundaries, preventing embrittlement [6,7].

Oxide dispersion strengthened (ODS) steels are fabricated by powder metallurgy routes. As a first step, the elemental or pre-alloyed powders are milled with Y_2O_3 powders. This process is followed by consolidation of the blend by hot extrusion or hot isostatic pressing (HIP). The consolidated billet is subsequently thermo-mechanically treated. The overall process determines the final microstructure, which may largely affect the mechanical performance of the steel.

The aim of this work is to investigate the microhardness, tensile, and fracture properties of a model ODS Fe–Cr alloy, and a reference non-ODS Fe–Cr alloy, in order to better understand the microstructural and tensile characteristics of more chemically complex ODS steels.

2. Experimental methods

The investigated alloys had nominal compositions of Fe–12 wt%Cr–0.4 wt%Y_2O_3 and Fe–12 wt%Cr for the ODS and non-ODS alloys, respectively. The alloys were produced by the following powder metallurgy route, as described in Ref. [8]: the Fe and Cr elemental powders were mechanically alloyed in an attritor ball mill until Cr was incorporated into the Fe lattice. For the ODS material, the alloyed powder was subsequently milled with 0.4 wt% of monoclinic Y_2O_3 nanometer-sized particles. The milled powder was consolidated by HIP at 1373 K and 190 MPa for 2 h.

Tensile tests were carried out in a temperature range of 298–973 K. Flat tensile test specimens with 20 mm gauge length, 3 mm width, and 1 mm thickness were obtained from the as-HIPed bars by electric discharge machining, and carefully ground and polished. Before testing, the samples were heat treated for 4 h at 1023 K in a vacuum of $\leqslant 10^{-5}$ Pa. Tensile tests at a constant cross-head rate of 0.1 mm/min were performed up to fracture in a Shimadzu AG-I universal testing machine equipped with a high precision load cell and a furnace. All tests above room temperature were carried out under flowing pure Ar. Three tests were performed for each temperature and alloy.

* Corresponding author. Tel.: +34 916249184; fax: +34 916248749.
E-mail address: vanessa.decastro@uc3m.es (V. de Castro).

Vickers microhardness measurements were also taken for the as-HIPed and heat treated ODS and non-ODS alloys, by applying a load of 300 g for 20 s onto mirror polished sample surfaces. The microhardness average value was determined from 10 different indentations, at least.

The fracture surfaces of the tested samples were investigated using a Philips XL-30 scanning electron microscope (SEM) operated at 20 kV and equipped with an X-ray energy dispersive spectrometer (XEDS).

3. Results and discussion

The microstructure of the ODS and non-ODS Fe12Cr alloys under study has been extensively characterized and is reported in Refs. [8–10]. The more relevant characteristics of the alloys can be summarized as follows: both ODS and non-ODS alloys present a similar microstructure, composed of martensite laths and a high density of dislocations in the as-HIPed state. The martensitic structure is related to the presence of ~0.09 wt% of C in the ODS alloy (and ~0.07 wt% in the non-ODS alloy). During the milling process, contamination from the grinding media and attritor parts is impossible to avoid, leading to C ingress. The grain structure was not completely recovered after heat treatment, exhibiting equiaxed morphology with grain sizes as large as ~1 μm on the recovered areas. Cr-rich precipitates, with sizes in the range 50 nm–1 μm and identified as $M_{23}C_6$ carbides and Cr_2O_3 oxides, were found in both alloys. For the ODS alloy, a barely homogeneous dispersion of Y-rich nanoparticles smaller than 40 nm in diameter was found. Some of these particles corre-sponded to Y_2O_3 and $YCrO_3$, but others could not be identified. In specific particles, a structure composed of a Y–O rich core with Cr-rich shell was evident.

3.1. Vickers microhardness

Table 1 presents the hardness values obtained for the Fe12Cr alloys in the as-HIPed and heat treated condition. The hardness values are remarkably higher for the as-HIPed alloys due to the presence of martensite and more dislocations in these alloys. Furthermore, the decrease in hardness after heat treatment in the non-ODS alloy is much more pronounced than in the ODS alloy, i.e., a decrease of ~46% compared with ~28%. This is attributed to the pinning effect of the nanoparticle dispersion that delays recovery and recrystallization. The heat treated ODS Fe12Cr alloy has microhardness values similar to the ones reported for Fe–(12–14)Cr–(0.1–0.3)Ti–0.3 Y_2O_3 steels consolidated by HIP and heat treated at 1123 K, see Ref. [11]. Forging before the heat treat-ment does not significantly change the microhardness, at least for the heat treated non-ODS Fe12Cr alloy, as the microhardness value is similar to the one found in a non-ODS Fe14Cr alloy forged at 1323 K and subsequently heat treated at 1123 K. When comparing the ODS counterparts, the microhardness value is ~8% lower in the ODS Fe12Cr than in the forged – heat treated ODS Fe14Cr alloy containing 0.3 wt%Y_2O_3 particles [12]. The higher homogeneity of the nanoparticle dispersion found in this ODS Fe14Cr alloy would account for the difference in hardness [10,13].

Table 1
Average microhardnesss values for the as-HIPed and heat treated ODS and non-ODS Fe12Cr alloys.

	as-HIPed (GPa)	Heat treated (GPa)
ODS/Fe12Cr	5.3 ± 0.3	3.83 ± 0.06
Fe12Cr	4.9 ± 0.2	2.63 ± 0.09

3.2. Tensile properties

Fig. 1 shows representative true stress–strain curves at all test temperatures for the ODS and non-ODS Fe12Cr alloys. The tensile characteristics of the alloys are summarized in Fig. 2. The yield strength (YS) and ultimate tensile strength (UTS) are significantly higher for the ODS alloy compared with non-ODS alloy, especially at lower temperatures. Considering that the grain sizes are similar in both alloys, and that the Cr-rich precipitates are also present in both cases, it should be concluded that this hardening is due to the Y-rich nanoparticle dispersion.

The UTS values for the ODS alloy at 298 and 673 K, which are marked with open symbols in the plot of Fig. 2b, are not real UTS values because the samples at these temperatures fractured before reaching the UTS. This early failure is attributed to the presence of Y-rich inclusions such as the one shown in the fracture surface presented in Fig. 3a. These inclusions, characterized in Section 3.3, were frequently found of the fracture surfaces of ODS samples.

For both alloys the YS and UTS decrease with increasing temperature, this decrease being steeper above 773 K. The ODS alloy presents YS and UTS values at RT that are superior to those of the non-ODS alloy in ~55% and 45%, respectively. It should be noted that the difference between the UTS of the alloys at low temperature may still be higher if the Y-rich inclusions mentioned above were not present in the samples. However, the differences in YS and UTS between the two alloys decrease with increasing temperature, the YS being ~24% higher, and the UTS ~47% at

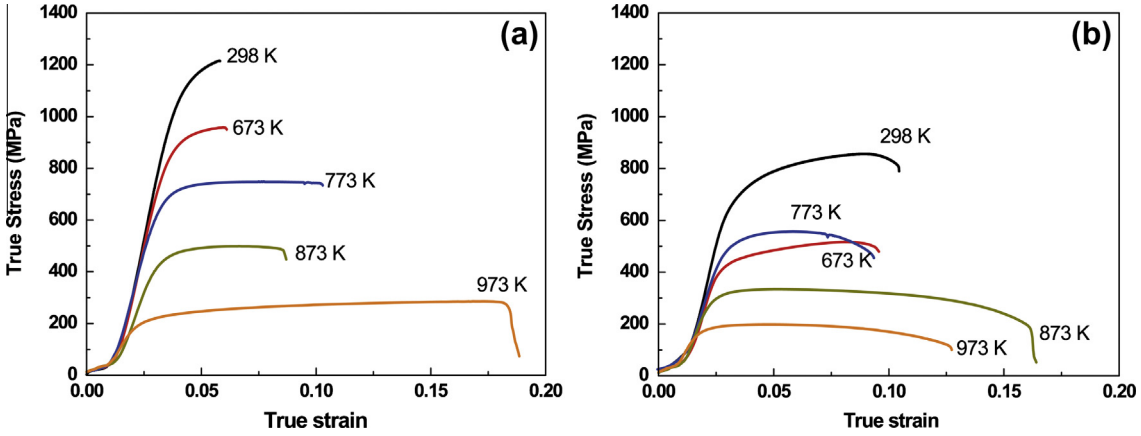

Fig. 1. Representative true stress–strain curves for the (a) ODS and (b) non-ODS Fe12Cr alloys.

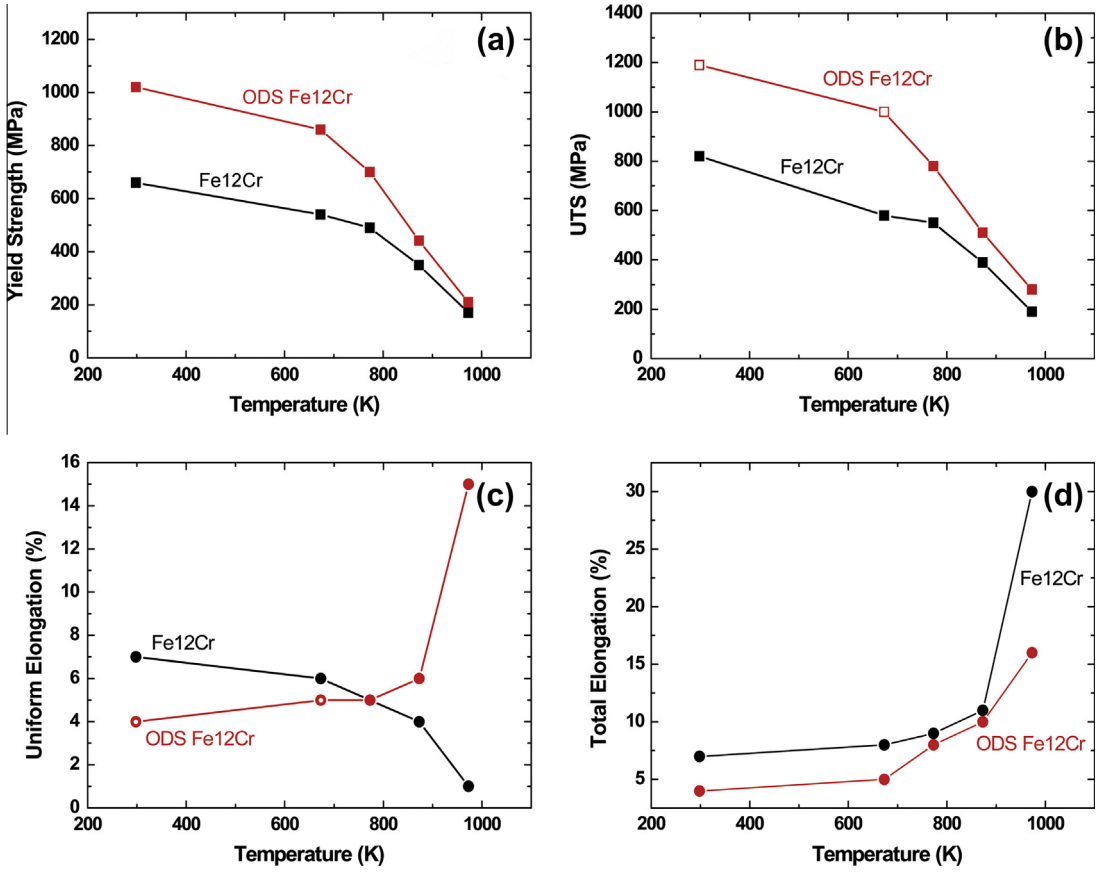

Fig. 2. Tensile properties for the heat treated ODS and non-ODS Fe12Cr alloys. The UTS and uniform elongation values represented with open symbols for the ODS alloy are actually the corresponding values at fracture.

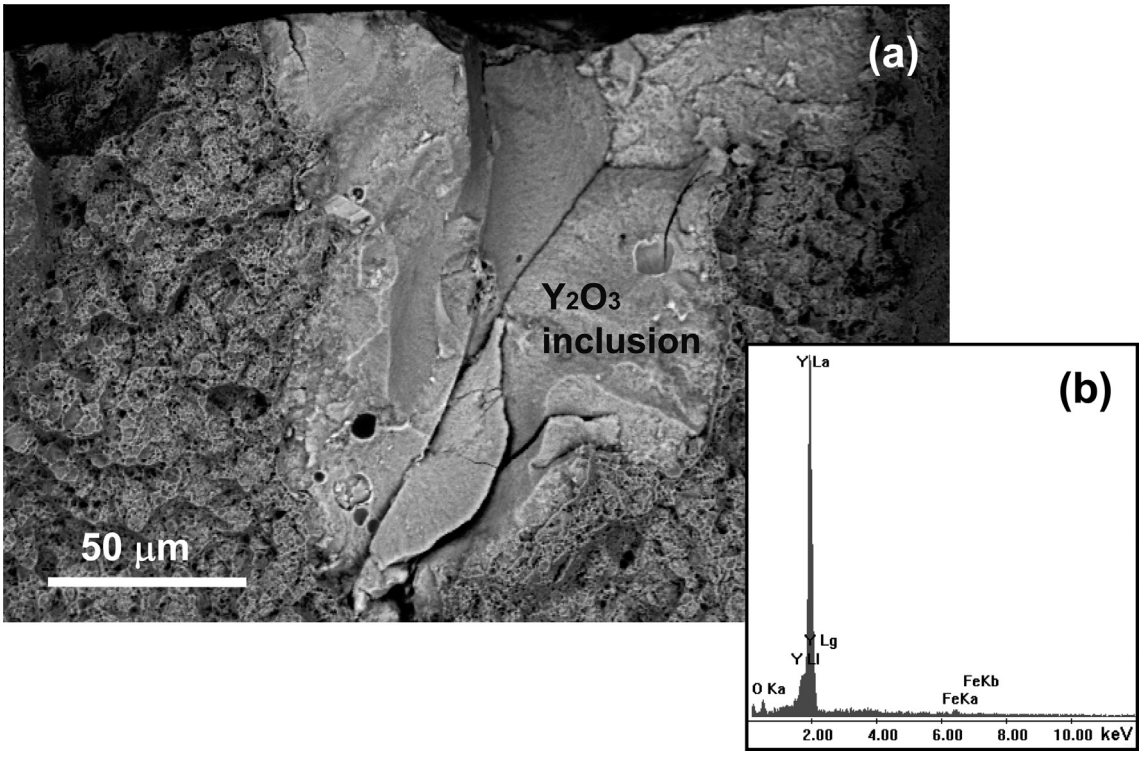

Fig. 3. (a) BSE-SEM micrograph of a Y-rich inclusion in the fracture surface of the ODS Fe12Cr alloy tested at 673 K. (b) XEDS spectrum of the Y-rich inclusion.

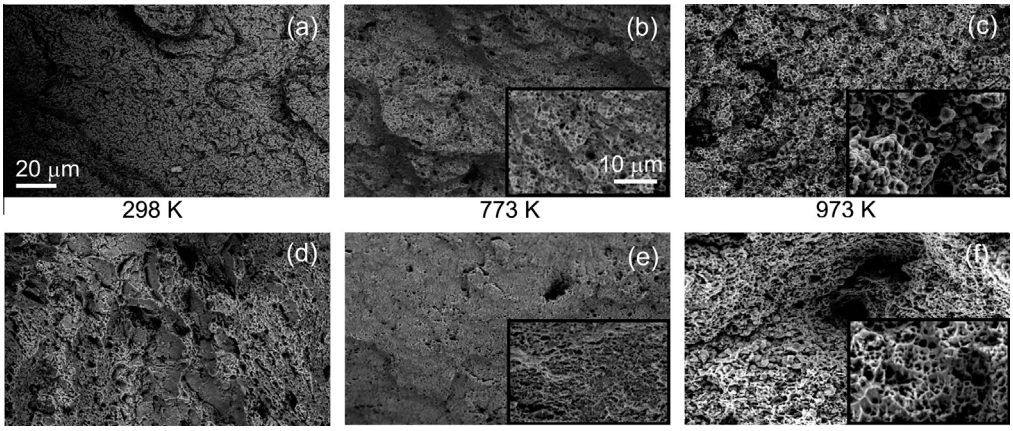

Fig. 4. Typical BSE-SEM fractographies of the tensile samples tested at different temperatures for (a–c) the ODS Fe12Cr and (d–f) the reference non-ODS. The insets in figures (b), (c), (e), and (f) show dimples on the fracture surfaces at higher magnification.

973 K. These results are in accordance with those reported for an as-HIPed ODS/Eurofer strengthened with 0.5 wt% Y_2O_3, in which the increase in UTS with respect to the base alloy is ~50% for temperatures below 973 K [14]. Moreover, the values obtained for the ODS Fe12Cr alloy are superior to the ones found in several ODS/Eurofer steels strengthened with 0.3 and 0.5 wt% Y_2O_3, at least for temperatures below 873 K [15]. However, the YS and UTS values obtained for the present model ODS Fe12Cr alloy are slightly smaller than the ones reported for the model ODS Fe14Cr alloy mentioned in Section 3.1 up to 973 K, and for Fe–12 wt%Cr–0.25 wt%Y_2O_3 alloy up to 773 K [12,16].

The relationships between the uniform and fracture elongations as a function of temperature are shown in Fig. 2c and d, respectively. It seems that the uniform elongation for the ODS alloy is smaller than the corresponding elongation for the non-ODS alloy up to temperatures of 773 K. However, failure of the ODS alloy before reaching the UTS occurs below 773 K, which impedes a reliable comparison. At higher temperatures, the uniform elongation for the ODS alloy increases drastically with temperature, in contrast to the non-ODS alloy. This is evidence that the ODS particles are sites for effective nucleation and pinning of dislocations with capability for inhibiting dynamical recovery and grain coarsening. The same trend has been recently observed on the model ODS Fe14Cr alloy mentioned above [12]. The fracture elongation for both alloys increases with increasing temperature, being especially higher for the non-ODS alloy at 973 K.

3.3. Fracture surface analyses

Representative SEM micrographs of the fracture surfaces of the ODS and non-ODS tensile specimens are shown in Fig. 4. Analyses of the fractographies indicate that the ODS alloy is less ductile than the non-ODS alloy at all temperatures. This is also inferred from Fig. 5, which shows that the ODS alloy presents a smaller reduction in area (RA) than the non-ODS alloy through the temperature range investigated. The ODS samples fail in a quasi-brittle mode at temperatures below 873 K (Fig. 4a and b), although the formation of dimples is apparent in some areas of the samples tested at 673 and 773 K, as shown in the inset of Fig. 4b. The brittleness of the ODS alloy is attributed to the presence of inclusions that promote a premature failure of the alloys, as shown in Fig. 3a. XEDS analyses show that these inclusions are Y-rich (Fig. 3b). It can be concluded from these observations that the initial Y_2O_3 powders formed aggregates, which could not be well dispersed during the milling process under the present conditions. The Y-rich inclusions with sizes on the order of 100 μm have often been observed on the fracture surfaces of the ODS specimens.

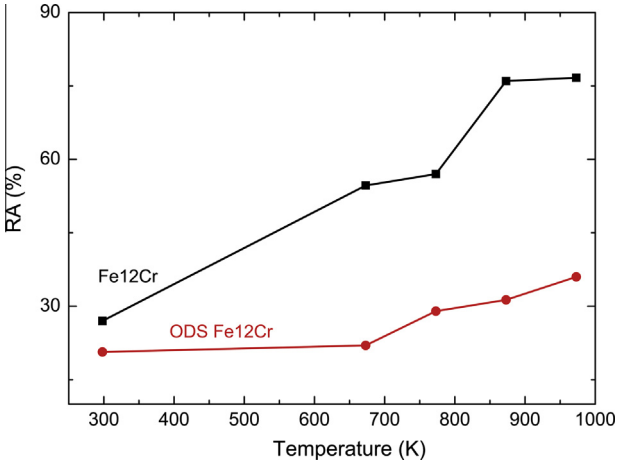

Fig. 5. Reduction in area of the fractured surfaces as a function of temperature for the ODS Fe12Cr and non-ODS alloys.

Profusion of dimpled areas at 973 K indicates the higher ductility found at this temperature, see Fig. 4c and f. This is also inferred from the higher RA, as Fig. 5 reveals.

4. Conclusions

The ODS Fe12Cr alloy exhibits yield and tensile strengths of 1020 and 1190 MPa, respectively, compared with values of 660 and 820 MPa for the non-ODS alloy. The strengthening effect of the oxide dispersion appears to be effective up to 973 K, at least. The SEM observations of fracture surfaces reveal that the ODS samples at temperatures below 873 K fail in a quasi-brittle mode, although the formation of dimples is apparent in some areas of the samples tested at 673 and 773 K. The reference non-ODS alloy exhibits similar fracture characteristics but with a clear profusion of dimpled areas at 673 and 773 K. The reduction of area at fracture for the ODS alloys ranges between 22% and 35% over the test temperature range in contrast with a variation of 28–75% for the reference non-ODS alloy.

Acknowledgements

The authors gratefully acknowledge the support provided by the Spanish Ministry of Science and Innovation (project ENE 2010-17462), the Comunidad de Madrid through the program

ESTRUMAT-CM (Grant S0505/MAT/0077) and the European Commission through the European Fusion Development Agreement.

References

[1] J.L. Boutard, A. Alamo, R. Lindau, M. Rieth, C. R. Phys. 9 (2008) 287.
[2] N. Baluc, R. Schäublin, P. Spätig, M. Victoria, Nucl. Fusion 44 (2004) 56.
[3] R.L. Klueh, D.R. Harries, High Chromium Ferritic and Martensitic Steels for Nuclear Applications, American Society for Testing and Materials, West Conshohocken, PA, USA, 2001.
[4] R. Lindau, A. Möslang, M. Schirra, P. Schlossmacher, M. Klimenkov, J. Nucl. Mater. 307–311 (2002) 769.
[5] A. Möslang, Proceedings of ITER, une étape majeure vers l'énergie de fusion nucleaire 1 (2007) 96.
[6] S. Ukai, M. Fujiwara, J. Nucl. Mater. 307–311 (2002) 749.
[7] G.R. Odette, M.J. Alinger, B.D. Wirth, Annu. Rev. Mater. Res. 38 (2008) 471.
[8] [8] V. de Castro, T. Leguey, A. Muñoz, M.A. Monge, R. Pareja, E.A. Marquis, S. Lozano-Perez, M.L. Jenkins, J. Nucl. Mater. 386–388 (2009) 449.
[9] V. de Castro, E.A. Marquis, S. Lozano-Perez, R. Pareja, M.L. Jenkins, Acta Mater. 59 (2011) 3927.
[10] V. de Castro, S. Lozano-Perez, E.A. Marquis, M.A. Auger, T. Leguey, R. Pareja, Mater. Sci. Technol. 27 (2011) 719.
[11] Z. Oksiuta, N. Baluc, Nucl. Fusion 49 (2009) 055003.
[12] M.A. Auger, T. Leguey, A. Muñoz, M.A. Monge, V. de Castro, P. Fernández, G. Garcés, R. Pareja, J. Nucl. Mater. 417 (2011) 213.
[13] V. de Castro, T. Leguey, M.A. Auger, S. Lozano-Perez, M.L. Jenkins, J. Nucl. Mater. 417 (2011) 217.
[14] R. Lindau, A. Möslang, M. Schirra, P. Scholossmacher, M. Klimenkov, J. Nucl. Mater. 307–311 (2002) 769.
[15] R. Schaeublin, T. Leguey, P. Spätig, N. Baluc, M. Victoria, J. Nucl. Mater. 307–311 (2002) 778.
[16] R.L. Klueh, J.P. Schingledecker, R.W. Swindeman, D.T. Hoelzer, J. Nucl. Mater 341 (2005) 103.